The Astrophysical Journal, 771:102 (7pp), 2013 July 10 doi:10.1088/0004-637X/771/2/102

TURBULENCE IN THE SUPERMODEL: MASS RECONSTRUCTION WITH NONTHERMAL PRESSURE FOR A1835

R. Fusco-Femiano[1] and A. Lapi[2,3]
[1] IAPS-INAF, Via Fosso del Cavaliere, I-00133 Roma, Italy
[2] Dip. Fisica, Univ. "Tor Vergata," Via Ricerca Scientifica 1, I-00133 Roma, Italy
[3] SISSA, Via Bonomea 265, I-34136 Trieste, Italy
Received 2013 January 28; accepted 2013 May 13; published 2013 June 21

ABSTRACT

The total mass derived from X-ray emission is biased low in a large number of clusters when compared with the mass estimated via strong and weak lensing. *Suzaku* and *Chandra* observations out to the virial radius report in several relaxed clusters' steep temperature gradients that on assuming pure thermal hydrostatic equilibrium (HE) imply an unphysically decreasing mass profile. Moreover, the gas mass fraction appears to be inconsistent with the cosmic value measured from the cosmic microwave background. Such findings can be interpreted as evidence for an additional nonthermal pressure in the outskirts of these clusters. This nonthermal component may be due to turbulence stirred by residual bulk motions of extragalactic gas infalling into the cluster. Here, we present a SuperModel analysis of A1835 observed by *Chandra* out to the virial radius. The SuperModel formalism can include in the equilibrium a nonthermal component whose level and distribution are derived imposing that the gas mass fraction ($f_{\rm gas}$) equals the cosmic value at the virial radius. Including such a nonthermal component, we reconstruct from X-rays an increasing mass profile consistent with the HE also in the cluster outskirts and in agreement at the virial boundary with the weak-lensing value. The increasing $f_{\rm gas}$ profile confirms that the baryons are not missing but located at the cluster outskirts.

Key words: cosmic background radiation – galaxies: clusters: individual (A1835) – X-rays: galaxies: clusters

Online-only material: color figures

1. INTRODUCTION

Clusters of galaxies formed from the collapse of primordial density fluctuations are powerful cosmological probes that mostly rely on their total virial mass. The traditional method to estimate $M(r)$ is based on the intracluster plasma (ICP) density and temperature profiles derived from the X-ray bremsstrahlung emission. These profiles allow us to solve the equation of hydrostatic equilibrium (HE) assuming spherical symmetry. Comparing with masses estimated via strong and weak lensing (Arnaud et al. 2007; Mahdavi et al. 2008; Lau et al. 2009; Zhang et al. 2010; Battaglia et al. 2012) has highlighted that the X-ray mass is biased low by a systematic ∼10%–20% even in relaxed clusters. These differences in mass values suggest the presence of a nonthermal gas pressure support that could resolve this discrepancy. On the other hand, simulations unanimously show the presence of gas motions driven by the inflow of material into the cluster from its environment, mergers, and the supersonic movements of galaxies through the ICP. These motions may cause the development of turbulence in the cluster outskirts with a deep impact on the physics of the ICP (Nagai et al. 2007a, 2007b; Shaw et al. 2010; Burns et al. 2010; Vazza et al. 2011; Rasia et al. 2012). In addition, the gas clumping, which may be important at large radii, can considerably underestimate the total mass (Nagai & Lau 2011; Simionescu et al. 2011; Eckert et al. 2013a; Vazza et al. 2013).

An incorrect estimate of the total mass implies an incorrect determination of the baryon fraction ($f_{\rm gas}$) in the ICP that contains most of the baryons in clusters. The remaining baryons ($f_{\rm stars}$) that represent a few percent of the total mass are in stars and intracluster light (Gonzalez et al. 2007; Giodini et al. 2009). The total baryon fraction ($f_b = f_{\rm gas} + f_{\rm stars}$) and its evolution with the redshift are used to constrain cosmological parameters since it is believed to be representative of the universe (e.g., White et al. 1993; Metzler & Evrard 1994; Ettori et al. 2009). Current studies have shown that the cluster baryon fraction f_b derived at r_{500} is lower than the ratio Ω_b/Ω_M measured from the cosmic microwave background (CMB) by several experiments (Afshordi et al. 2007; Umetsu et al. 2009; Vikhlinin et al. 2006; Arnaud et al. 2007; Sun et al. 2009; Komatsu et al. 2011) raising the question of where the missing baryons are allocated (Rasheed et al. 2010). To address this issue, Landry et al. (2012) recently used *Chandra* X-ray observations to measure the gas mass fraction for a complete sample of massive clusters in the redshift range 0.15–0.30 from the *brightest cluster sample* (Ebeling et al. 1998; Dahle 2006). These clusters are observed at the radius within which the mass density is 500 times the critical density of the universe at the cluster's redshift. They find that the baryon content in these high-luminosity clusters is consistent at r_{500} with the cosmic ratio $\Omega_b/\Omega_M = 0.167 \pm 0.006$ implying that there are no missing baryons within this radius in the most luminous and massive clusters. However, in accord with several studies, they measure an increase of $f_{\rm gas}$ with radius raising the question of what happens to the gas mass fraction beyond r_{500}. It can be presumed that $f_{\rm gas}$ increases in going toward the virial boundary, as also reported by recent *Suzaku* observations (e.g., Simionescu et al. 2011). However, Landry et al. (2012) doubt the validity of this extrapolation considering that the gas could not be in HE beyond r_{500}, and/or that the clumping of the gas may always be more important toward the virial radius. An underestimate of the total mass may be the cause of the discrepancy between f_b and the ratio Ω_b/Ω_M at $r > r_{500}$.

One of the clusters in the sample of Landry et al. (2012) is A1835 ($z = 0.253$) which has been investigated by Bonamente et al. (2013) out to the virial radius due to a long exposure and

high-quality data. *Chandra* reports soft X-ray surface brightness emission out to a radial distance of ∼2.4 Mpc and a very steep temperature profile similar to that observed by *Suzaku* in some relaxed clusters (Bautz et al. 2009; Hoshino et al. 2010; Kawaharada et al. 2010; Walker et al. 2012b). This temperature profile implies a decreasing total mass profile at $r > r_{500}$, an f_b value consistent with the cosmological ratio at r_{500}, but inconsistent at greater distances. Their conclusion is that the steepening of the temperature profile is incompatible with the HE in the outskirts of the cluster as confirmed by recent *Suzaku* observations out to the virial radius (Ichikawa et al. 2013). Besides, Bonamente et al. (2013) report that a negative entropy gradient renders the ICP convectively unstable, flattening within a few Gyr the temperature profile for the transport of central hotter gas in the periphery of the cluster. They suggest the presence of cool gas in the outskirts of the cluster which may be the result of infall from the filamentary structure if this gas lies in projection against the outermost regions.

Here, we show how it is possible to reconstruct the total cluster mass using the SuperModel (Cavaliere et al. 2009) which includes a nonthermal pressure component (Cavaliere et al. 2011) due to turbulent motions. This component, in addition to the ICP thermal pressure, sustains the HE. Turbulence is related to the weakening of the accretion shocks which induces an increase of the bulk inflow energy in the cluster outskirts and also the saturation of entropy production determining the observed steep temperature profiles (see Lapi et al. 2010). In particular, we analyze A1835 showing that the inclusion of this nonthermal component also provides an increasing total mass in the cluster outskirts and in agreement with the weak-lensing measurements. The level and distribution of this nonthermal pressure support are obtained imposing that the baryon mass fraction is consistent with the cosmic ratio at the virial boundary (see Section 3).

Throughout the paper we adopt the standard flat cosmology with parameters $H_0 = 70$ km s^{-1} Mpc^{-1}, $\Omega_\Lambda = 0.7$, and $\Omega_M = 0.3$ (see Komatsu et al. 2011; Hinshaw et al. 2013; Planck Collaboration 2013a). With this, 1 arcmin corresponds to 237.48 kpc.

2. TURBULENCE IN THE SUPERMODEL

The wealth of current and upcoming data for emission in X-rays and scattering in the microwaves of the CMB photons for the Sunyaev–Zel'dovich (1980; SZ) effect requires a precision modeling of the ICP density $n(r)$ and temperature $T(r)$ distributions. This modeling is provided by the SM based on the run of the ICP specific *entropy* (adiabat) $k = k_B T/n^{2/3}$ set by the processes for its production and erosion. Active galactic nucleus (AGN) outbursts and deep mergers often followed by inner sloshing determine a rise of the entropy at the cluster centers; in addition there the entropy may be partly eroded by cooling processes. At the other end, a large quantity of entropy is continuously produced at the virial boundary R, where the ICP is shocked by the supersonic gravitational inflow of gas accreted from the environment along with the dark matter (DM), and is adiabatically stratified into the DM potential well. These physical processes concur to create a spherically averaged profile for the ICP entropy $k(r) = k_c + (k_R - k_c)(r/R)^a$; see Voit (2005). A central floor k_c (≈10–100 keV cm^2) is followed by an outer ramp with slope $a \approx 1$ (Tozzi & Norman 2001), leading to entropy values $k_R \sim$ some 10^3 keV cm^2 at the virial boundary.

The thermal pressure $p(r) \propto k(r)n^{5/3}(r)$ is used in the SM to balance the DM gravitational pull $-GM(< r)/r^2$ and sustain the HE out to the virial boundary. From the HE equation, we directly derive the temperature profile:

$$\frac{T(r)}{T_R} = \left[\frac{k(r)}{k_R}\right]^{3/5} \left\{1 + \frac{2}{5} b_R \int_r^R \frac{dx}{x} \frac{v_c^2(x)}{v_R^2} \left[\frac{k_R}{k(x)}\right]^{3/5}\right\}. \quad (1)$$

Note that the density follows $n(r) = [k_B T(r)/k(r)]^{3/2}$, so that $T(r)$ and $n(r)$ are linked, rather than independently rendered with multi-parametric expressions as in other approaches. The few physical parameters specifying $k(r)$ are enough to provide remarkably good fits to the detailed X-ray data on surface brightness and on temperature profiles of many cool-core (CCs) and non-cool-core clusters (see Fusco-Femiano et al. 2009), and to the SZ *Planck* profile for the Coma cluster (Fusco-Femiano et al. 2013). Good fits have been also obtained for the steep temperature profiles observed by *Suzaku* out to the virial radius in some relaxed CC clusters that, as suggested by Lapi et al. (2010), can be explained in terms of the entropy profile flattening observed in these clusters. The entropy run starts with an initial slope a, but for $r > r_b$ it deviates downward from a simple power law (see Equation (4) in Lapi et al. 2010) where r_b is a free parameter. The outer branch of the entropy profile is described by a linear decline of the slope with gradient $a' \equiv (a - a_R)/(R/r_b - 1)$. This lower entropy production may be explained in terms of decreasing accretion rate due to the slowdown at later cosmic times of the cosmological structure growth in an accelerating universe. The effect is enhanced by little mass available for accretion in cluster sectors adjacent to low-density regions of the surrounding environment. Thus, we expect azimuthal variations of the X-ray observables (Lapi et al. 2010).

This scenario seems to be confirmed by a recent analysis of a sample of relaxed CC clusters at redshift below 0.25 (Walker et al. 2012b). On the other hand, the clumping effect reported by numerical simulations (Nagai & Lau 2011) is not large enough to account for the observed amount of entropy flattening. Also, the proposed difference between the electron and ion temperatures in the ICP inside the accretion shock in the outskirts as a cause of the entropy profile flattening (Hoshino et al. 2010; Akamatsu et al. 2011) seems to be in contrast with SZ effect observations with *Planck* (Planck Collaboration 2013b).

The weakening of the accretion shock in relaxed clusters not only reduces the thermal energy to feed the intracluster entropy, but also increases the amount of bulk energy to drive turbulence into the outskirts (Cavaliere et al. 2011). Turbulent motions start the virial radius R with coherence lengths $L \sim R/2$ set in relaxed CC clusters by the pressure scale height or by shock segmentation (see Iapichino & Niemeyer 2008; Valdarnini 2011; Vazza et al. 2010). Then they fragment downstream into a dispersive cascade to sizes l. Larger values of turbulent energy compared to the gas thermal energy are reported by simulations in the innermost cluster regions of post-merger and merging clusters. Here instead we deal with the outskirts of relaxed clusters where the simulations report much lower values in the cluster cores but an increasing $E_{\rm turb}/E_{\rm thermal}$ profile going toward the virial radius (e.g., Vazza et al. 2011).

Since turbulent motions contribute to the pressure to sustain HE, we focus on the ratio $\delta(r) \equiv p_{\rm nth}/p_{\rm th}$ of turbulent to thermal pressure with radial shape decaying on the scale l from the boundary value δ_R. The total pressure is now $p_{\rm tot}(r) = p_{\rm th}(r) + p_{\rm nth}(r) = p_{\rm th}(r)[1 + \delta(r)]$, which, when inserted in the

HE equation, gives the temperature profile in the form

$$\frac{T(r)}{T_R} = \left[\frac{k(r)}{k_R}\right]^{3/5}\left[\frac{1+\delta_R}{1+\delta(r)}\right]^{2/5} \times \left\{1 + \frac{2}{5}\frac{b_R}{1+\delta_R}\int_r^R \frac{dx}{x}\frac{v_c^2(x)}{v_R^2}\left[\frac{k_R}{k(x)}\right]^{3/5}\left[\frac{1+\delta_R}{1+\delta(x)}\right]^{3/5}\right\}. \quad (2)$$

Again, $n(r)$ is linked to $T(r)$ by $n(r) = [k_B T(r)/k(r)]^{3/2}$. In our numerical computations, we adopt the functional shape

$$\delta(r) = \delta_R e^{-(R-r)^2/l^2} \quad (3)$$

which decays on the scale l inward of a round maximum. The runs $\delta(r)$ we adopt are consistent with those indicated by numerical simulations (Lau et al. 2009; Vazza et al. 2011). A power law has instead been used to describe the radial distribution of the fraction $p_{\rm nth}/p_{\rm tot}$ by Morandi et al. (2012; see also Shaw et al. 2010) in their three-dimensional structure reconstruction of A1835. They performed a triaxial joint analysis using X-rays, and strong lensing (SL) and SZ data available to infer the gas entropy and the nonthermal pressure profiles out to r_{200}.

3. SUPERMODEL ANALYSIS OF A1835

The SM analysis of A1835 observed by *Chandra* (Schmidt et al. 2001; Bonamente et al. 2013) begins assuming that the total pressure for the HE is given only by the thermal ICP pressure (see Equation (1)). Figure 1 shows the fit to the projected temperature profile (blue line) assuming a deviation of the entropy from the profile $k \sim r^a$ at $r > r_b$; this because a power-law increase is inconsistent with the *Chandra* data (see the green line). From the surface brightness distribution (see Figure 1), we derive the ICP density profile of Figure 2 in a slightly different way than the deprojected electron density profile obtained by Li et al. (2012) from *Chandra* observations and in agreement with the profile derived at $r \gtrsim 180''$ by the *Suzaku* observations (Ichikawa et al. 2013). As shown in Figure 5, the gas density profile gives a central SZ effect value absolutely consistent with the observations (Reese et al. 2002), at variance with the gas density profile derived by Li et al. (2012). Moreover, our SZ effect profile reproduces fairly well the profile observed by Bolocam at $r \gtrsim 30''$ (Sayers et al. 2011). The central gas density is 0.49 ± 0.03 cm^{-3} while at the virial boundary ($R =$ 2.4 Mpc or 606.4 arcsec) it is $(5.73 \pm 0.37) \times 10^{-5}$ cm^{-3}. This last value is about a factor of two greater than the gas density reported by Morandi et al. (2012) at the virial radius. In accord with Bonamente et al. (2013), who analyzed the *Chandra* data with the fitting formulae of Vikhlinin et al. (2006), the steep temperature profile causes a decreasing total matter at $r \gtrsim 400''$ and a consequent gas mass fraction consistent with the cosmic value at $r = r_{500}$ ($\approx 327''$), but absolutely inconsistent at larger radii (see Figure 3). This $M_{\rm tot}$ profile provides evidence that beyond r_{500} the HE is not supported only by thermal pressure, as suggested by several theoretical studies (e.g., Lau et al. 2009).

In Section 2, we have shown that the SM formalism has the ability to straightforwardly include in the equilibrium a nonthermal pressure to yield the total pressure $p_{\rm tot} = p_{\rm th}(1+\delta)$ where the pressure $p_{\rm nth} = p_{\rm th}\delta$ can be physically characterized in terms of a normalization provided by the infall kinetic energy seeping through the virial shocks to drive turbulence, and of a dissipative decay scale (see Equations (2) and (3)). The inclusion

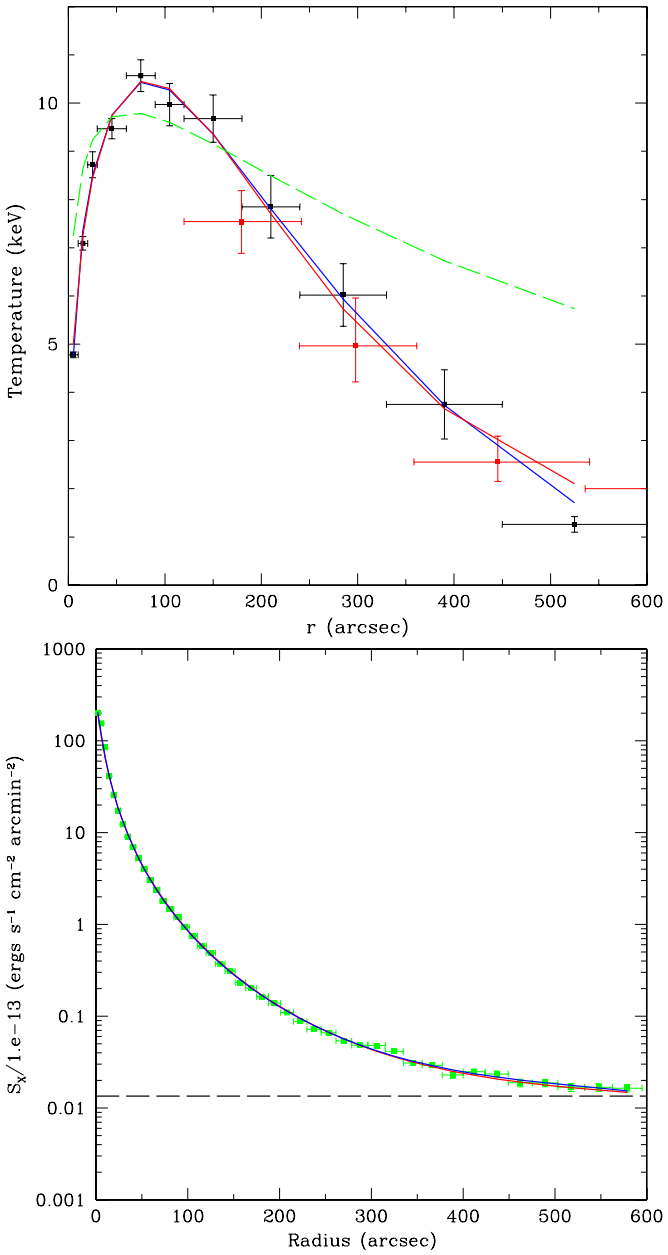

Figure 1. Top panel: projected temperature profile (black points) observed by *Chandra* in A1835 (Bonamente et al. 2013); red points are by *Suzaku* (Ichikawa et al. 2013). The blue line is the SM fit with $\delta(r) = 0$ (see Equation (1)); the red line is the SM fit with $\delta_R = 1.4$ and $l = 0.5$ (see Equations (2) and (3)); the green line is the fit without imposing the entropy flattening at $r > r_b$ (see the text). Bottom panel: exposure corrected surface brightness profile of A1835 in the X-ray band (0.7–2 keV) observed by *Chandra*; the dashed line is the background level (Bonamente et al. 2013); the blue line is the SM fit with $\delta(r) = 0$ (see Equation (1)); the red line is the SM fit with the above values of δ_R and l.

(A color version of this figure is available in the online journal.)

of a nonthermal component leads to an increasing total mass also in the more peripheral regions of A1835 (see Figure 3, red line). We determine the quantities δ_R and l (see Equation (3)) imposing that the baryon mass fraction equals the cosmic value at the virial radius (red line in Figure 3), and that the mass profile is smooth in the outskirts. These values yield the pressure profiles $p_{\rm th}$, $p_{\rm nth}$, and $p_{\rm tot}$ shown in Figure 5 ($\delta_R = 1.4$, $l = 0.5R$). The thermal pressure is about 40% of the total pressure at the virial radius helped by turbulent motions in sustaining the equilibrium, while it predominates at the center. The nonthermal pressure becomes

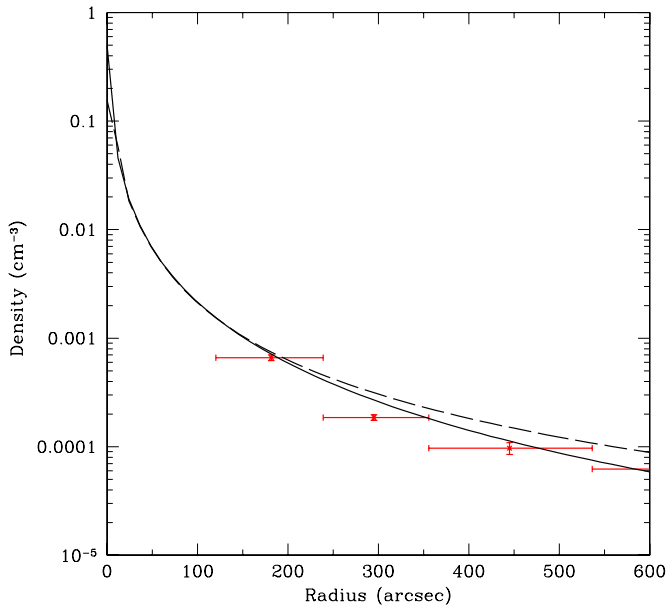

Figure 2. ICP density profile. The solid line is the electron density profile obtained by the SM fit to the surface brightness profile observed by *Chandra* in A1835 (see Figure 1); the dashed line is the fit with a double-β model (Cavaliere & Fusco-Femiano 1976) of the deprojected density derived by Li et al. (2012) from the *Chandra* results. The red points are the *Suzaku* results (Ichikawa et al. 2013).

(A color version of this figure is available in the online journal.)

significant at $r \gtrsim 400''$ where our analysis with $\delta = 0$, in accord with Bonamente et al. (2013), reports a decreasing mass profile.

In the presence of a nonthermal pressure, the traditional equation to estimate the total mass $M(r)$ within r is modified as

$$M(r) = -\frac{k_B[T(r)(1+\delta(r)]r^2}{\mu m_p G} \times \left\{\frac{1}{n_e(r)}\frac{dn_e(r)}{dr} + \frac{1}{T(r)[(1+\delta(r)]}\frac{dT(r)[1+\delta(r)]}{dr}\right\} = -\frac{k_B[T(r)(1+\delta(r)]r^2}{\mu m_p G} \times \left[\frac{1}{n_e(r)}\frac{dn_e(r)}{dr} + \frac{1}{T(r)}\frac{dT(r)}{dr} + \frac{\delta(r)}{1+\delta(r)}\frac{2}{l^2}(R-r)\right], \quad (4)$$

where k_B is the Boltzmann constant, μ is the mean molecular weight, m_p is the proton mass, and G is the gravitational constant. The mass of the hot gas is

$$M_{\rm gas} = 4\pi\mu_e m_p \int n_e(r) r^2 dr,$$

where μ_e is the mean molecular weight of the electrons.

The fit to the *Chandra* projected temperature profile with the ratio $\delta = p_{\rm nth}/p_{\rm th} > 0$ is only slightly different from the fit with only the thermal pressure to sustain the HE. This difference is completely negligible in the fit to the brightness profile due to its weak dependence on the temperature (see Figure 1). From these fits, we extract values (with their 1σ uncertainty) of the parameters $k_c \approx 5 \pm 2$ keV cm^2, $a \approx 1.29_{-0.48}$, and $k_R \approx 1040 \pm 520$ keV cm^2 specifying the entropy pattern for $r \leqslant r_b$; for $r > r_b$ the entropy decline starts at $r_b \approx 0.11^{+0.16} R$ ($\approx 260^{+380}$ kpc), with a gradient $a' \approx 0.47_{-0.33}$. Figure 4 shows the three-dimensional temperature and entropy profiles of the

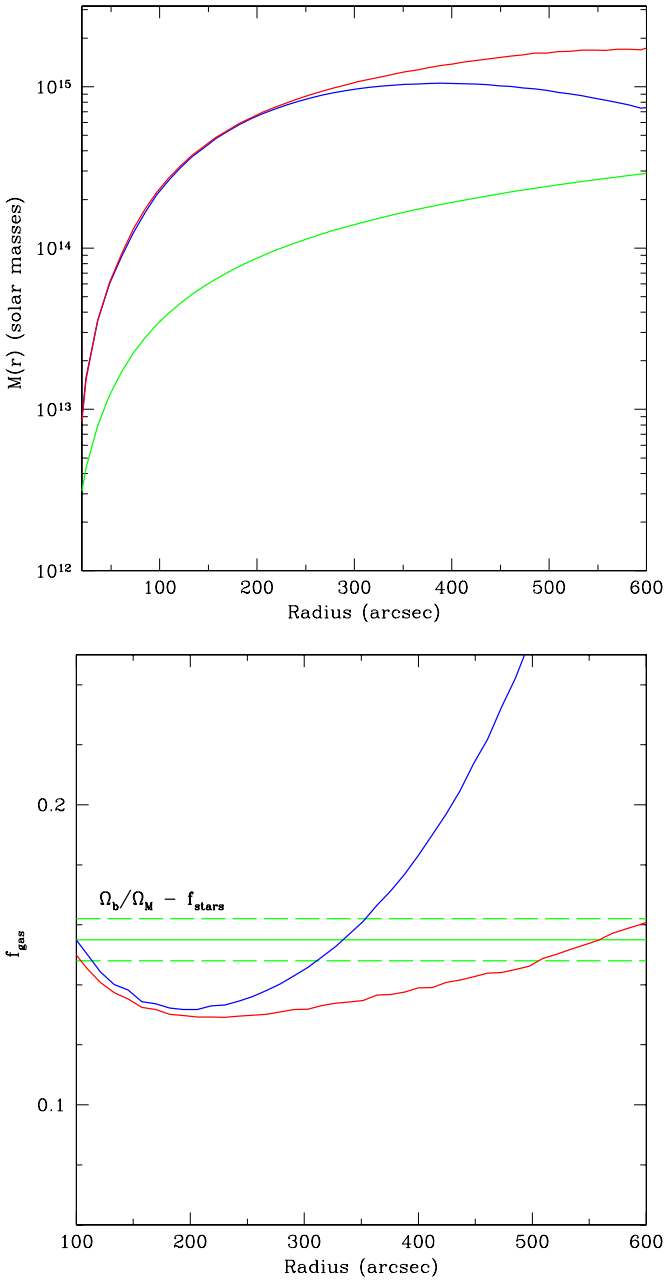

Figure 3. Top panel: total cluster mass and ICP mass for A1835 derived from the SM analysis. The blue line is the total mass obtained with $\delta(r) = 0$ (see Equation (4)); the red line is the total mass derived with $\delta_R = 1.4$ and $l = 0.5$ (see Equations (3) and (4)); the green line is the gas mass derived from the gas density of Figure 2 (solid line, central value $n_{e,0} = 0.49$ cm^{-3}). Bottom panel: gas mass fraction derived from the above mass profiles; the blue line is with $\delta(r) = 0$; the red line is with the above values of δ_R and l; green lines are the difference of the cosmic baryon fraction and the fraction of baryons in stars and galaxies, $\Omega_b/\Omega_M - f_{\rm stars} = 0.155 \pm 0.007$ (Komatsu et al. 2011; Gonzalez et al. 2007).

(A color version of this figure is available in the online journal.)

ICP when a nonthermal pressure component is included in the HE equation. Our entropy profile for $\delta > 0$ is consistent with the observed entropy values derived by *XMM-Newton* (Zhang et al. 2007) and *Suzaku* (Ichikawa et al. 2013) observations. Our value of r_b between $\approx$ 260 and 640 kpc derived by *Chandra* observations is consistent with the radius in the interval $\approx$470–950 kpc where the *Suzaku* entropy profile starts to decline downward (see Figure 7 in Ichikawa et al. 2013). We also note

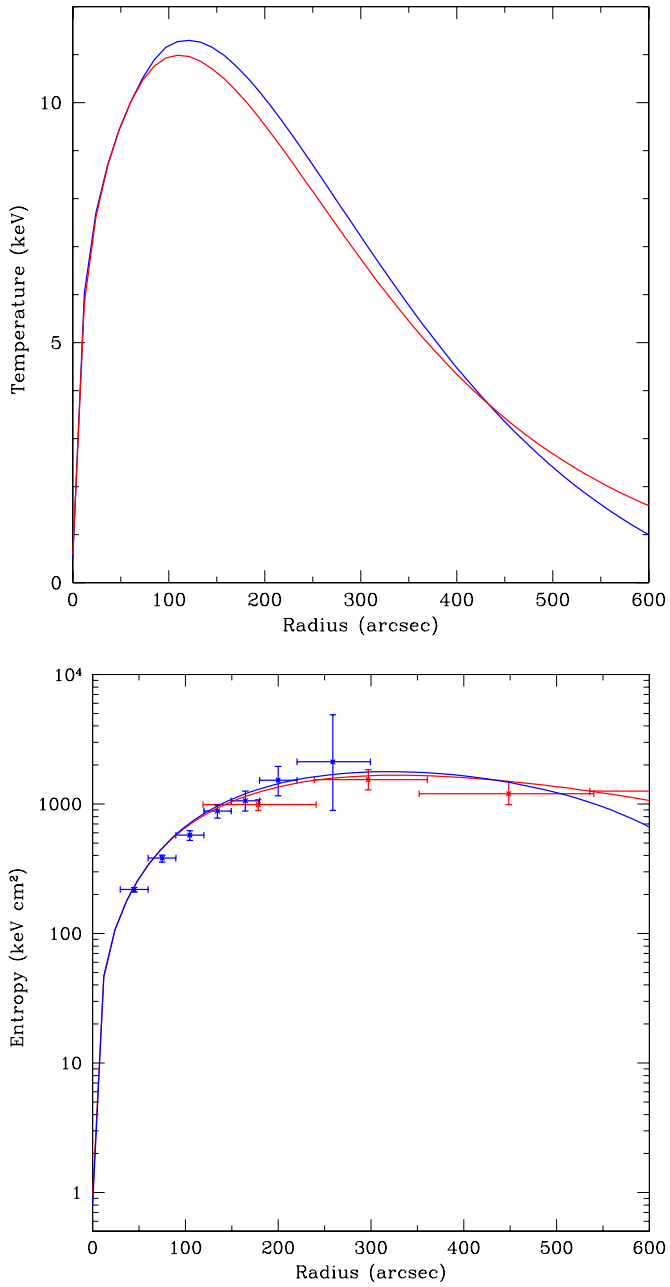

Figure 4. Top panel: radial temperature profile. The blue line is the radial temperature obtained by the SM fit with $\delta(r) = 0$ to the projected profile observed by *Chandra* in A1835 (see Figure 1); the red line is from the SM fit with $\delta_R = 1.4$ and $l = 0.5$. Bottom panel: SM entropy profile of A1835. The blue points are reported by *XMM-Newton* (Zhang et al. 2007); the red points are from *Suzaku* (Ichikawa et al. 2013). The blue line is with $\delta(r) = 0$; the red line is with $\delta_R = 1.4$ and $l = 0.5$.

(A color version of this figure is available in the online journal.)

that the SM entropy profile (red line) is sufficiently flat to satisfy the Schwarzschild criterion discussed by Bonamente et al. (2013) for the convective instability. Moreover, an increasing entropy profile that deviates from a power law is within the uncertainty of the slope a'.

4. DISCUSSION AND CONCLUSIONS

Only recently has the use of the *Suzaku* observations and of the SZ effect profiles allowed us to obtain some first insights on the thermodynamic properties of the cluster outskirts. This avoids resorting to extrapolations of the information available at $r \lesssim r_{500}$ to estimate the ICP and total masses going toward the virial boundary. The *Suzaku* and *Chandra* observations of several relaxed clusters have highlighted steep temperature profiles and entropy profiles that deviate from the expected power-law increase (e.g., Walker et al. 2012b). However, a recent combined analysis of SZ and X-ray data does not seem to indicate the entropy flattening in relaxed clusters (Eckert et al. 2013b). As already reported in Lapi et al. (2010) for a number of clusters, here we confirm for A1835 that the observed steep temperature profile measured with *Chandra* can be fitted by our SM only imposing a deviation of the entropy profile from a power-law increase at $r > r_b$. Also, the recent *Suzaku* observations (Ichikawa et al. 2013) report an entropy flattening; a similar behavior is found in the combined X-rays, and SL, and SZ data analysis of Morandi et al. (2012). We highlight that the goodness of our gas density and temperature profiles obtained by the SM fits to the *Chandra* X-ray observables is widely tested. The derived entropy profile is in agreement with the entropy values reported by *XMM-Newton* and *Suzaku* results (see Figure 4), and the SZ effect profile is consistent with the observations (see Figure 5).

In the Perseus cluster, observed by *Suzaku* in the outskirts, the gas mass fraction exceeds at the virial boundary the cosmic baryon value measured by the CMB (Simionescu et al. 2011). The authors suggest that the most plausible explanation for this apparent baryon excess toward the cluster periphery is gas clumping. According to this interpretation, the electron density is overestimated affecting gas mass fraction, entropy, and pressure profiles. The observed electron density must reach a value of up to ∼4 of the true density at the virial radius to have $f_{\rm gas}$ consistent with the cosmic value. However, as reported by Walker et al. (2012a, 2012b) the gas clumping derived by Nagai & Lau (2011) appears insufficient to match observations and is expected to be most significant at $r \gtrsim r_{200}$ while the observed entropy profiles start to flatten around $0.5r_{200}$ (see also Ichikawa et al. 2013). However, a recent paper by Walker et al. (2013) attributes to the gas clumping the major responsibility of the entropy flattening observed in several clusters. However, for A1835 the observed density needs to be overestimated by a large factor ∼7 to make the entropy profile agree with a power-law increase in the outskirts. Besides, the measured temperatures are too low compared to predictions and seem to be responsible for the entropy flattening in this cluster.

The observed sharp drops in temperature imply decreasing mass profiles in the outskirts of some relaxed galaxy clusters (e.g., Kawaharada et al. 2010; Bonamente et al. 2013; Ichikawa et al. 2013). This unphysical situation may be interpreted in terms of an ICP far from the HE. However, simulations show that clusters are subject to an intense activity from the surrounding cluster environment. Continued infall of gas onto clusters along filaments, violent mergers of groups and subclusters, and supersonic motions of galaxies through the ICP may induce turbulence that gives rise to a nonthermal pressure (Lau et al. 2009; Burns et al. 2010; Vazza et al. 2011). The weakening of the accretion shocks not only lowers the entropy production but also increases the amount of bulk energy to drive turbulence into the outskirts (Cavaliere et al. 2011). The result is that in addition to the thermal pressure a nonthermal component may sustain the HE to obtain an increasing mass profile and therefore a more accurate determination of the baryon gas fraction.

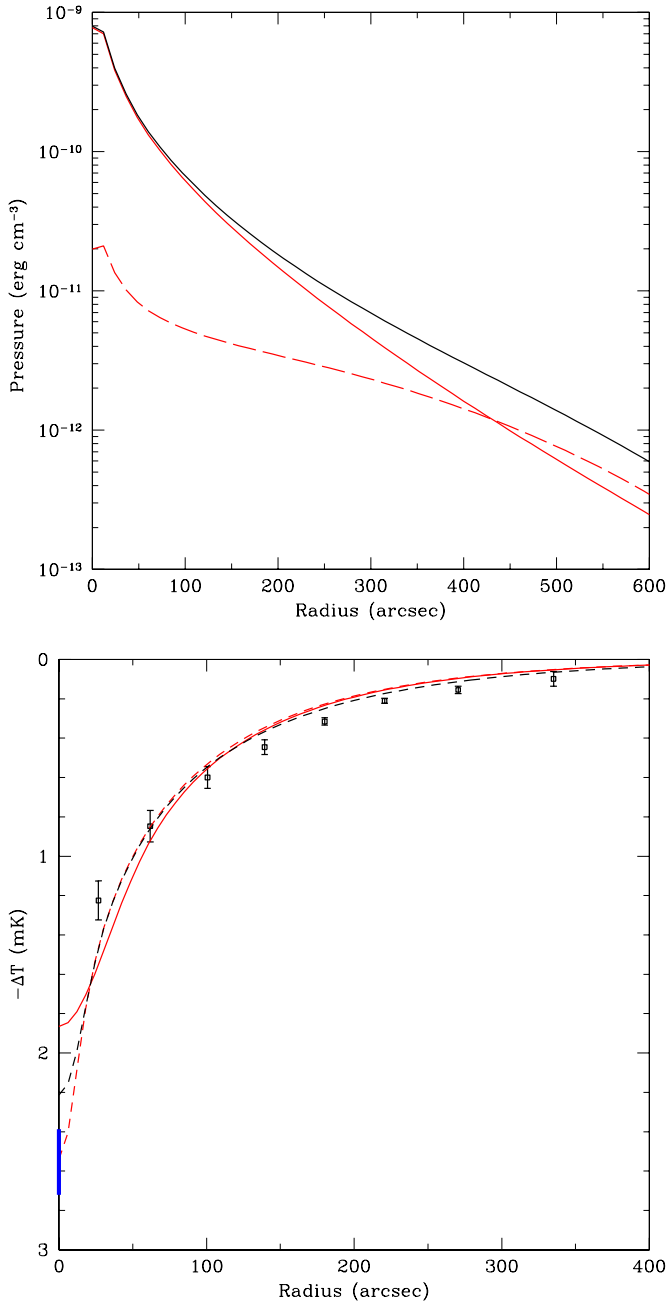

Figure 5. Top panel: pressure profiles. The red line is the thermal pressure; the dashed line is the nonthermal pressure; the black line is the total pressure ($p_{\rm tot} = p_{\rm th} + p_{\rm nth}$). Bottom panel: the SZ effect in A1835. The dashed red line is the SZ effect profile obtained with the ICP density profile of Figure 2 (solid line) and temperature profile of Figure 4 (red line, $\delta > 0$); the dashed black line is the SZ effect profile obtained with the gas density profile (dashed line of Figure 2) derived by Li et al. (2012) and temperature profile of Figure 4 (red line). These two profiles are compared with the central SZ effect value ($2.502^{+0.150}_{-0.175}$ mK, blue point) obtained by the OVRO/BIMA interferometers with resolution 18″ (Reese et al. 2002). The red line is the SZ effect profile obtained with the ICP density profile of Figure 2 (solid line) and temperature profile of Figure 4 (red line, $\delta > 0$) to compare with the black points observed by *Bolocam* at 58″ resolution (Sayers et al. 2011). All these profiles and the data have been scaled to a frequency dependence of -2 of the thermal SZ effect.

(A color version of this figure is available in the online journal.)

We test this possibility in A1835, observed by *Chandra* out to a radial distance of ∼2.4 Mpc, exploiting the SM formalism; the latter is able to include a nonthermal component (see Equation (2)), at variance with the fitting formulae used in the analysis of the cluster X-ray observables by Bonamente et al. (2013) and Landry et al. (2012). To determine the level and distribution of the nonthermal pressure, which, in addition to the thermal pressure, sustains the HE, we have imposed that the gas baryon fraction equals the observed cosmic value at the virial radius R. Our constraint is supported by the *Suzaku* observations that report a gas mass fraction, defined by the lensing total mass, which at R agrees with the cosmic baryon fraction. Also, the combined analysis of Eckert et al. (2013a) reports that at r_{200} the gas fraction converges for relaxed clusters to the expected value.

The thermal and nonthermal pressure profiles of Figure 5 define the total pressure distribution that guarantees HE everywhere as evidenced by the increasing profile of the cluster mass (see Equation (2) and Figure 3). The goodness of the SM analysis is confirmed by the comparison between our total mass values at r_{500} and R with the weak-lensing cluster mass measured by Clowe & Schneider (2002) and Hoekstra et al. (2012). In particular, the latter authors report $M_{\rm vir}^{\rm NFW} = 1.89^{+0.38}_{-0.35} \times 10^{15}\, M_\odot$ consistent with our value of $\sim 1.75 \times 10^{15}\, M_\odot$ obtained with $\delta > 0$ and inconsistent with the value of $\sim 7.50 \times 10^{14}\, M_\odot$ derived when the HE is supported only by the thermal pressure ($\delta = 0$).

For A1835, we obtain a nonthermal pressure contribution at the virial radius around 60% of the total pressure and $l \sim 0.5R$ in agreement with the simulations of Burns et al. (2010) which report $p_{\rm nth}/p_{\rm tot} \approx$ 60%–65% for a sample of clusters. The ratio between the mass estimated including turbulence in the SM and the mass estimated without turbulence $M_{\rm turb}/M_{\rm noturb}$ is ∼2.4. P. A. Giles et al. (2013, in preparation) found that X-ray hydrostatic masses for relaxed clusters are underestimated by a factor 1.21 ± 0.23 when compared to the weak-lensing masses. The level of the nonthermal pressure at the virial radius and the ratio $M_{\rm turb}/M_{\rm noturb}$ are strictly related to the ICP temperature run that is mainly responsible for the mass profile. The above values are justified by the uncommon drop of a factor ∼10 from the peak temperature to the value at the virial radius reported by *Chandra* in A1835 (see Figure 1). A lower value (∼5) is reported by *Suzaku* (Ichikawa et al. 2013). For a drop factor of ∼2.5, more similar to those reported by *Suzaku* observations in other clusters, we find that the nonthermal pressure at the virial radius decreases to ∼35% of the total pressure and $M_{\rm turb}/M_{\rm noturb}$ lowers to ∼1.31 consistent with the average value derived by P. A. Giles et al. (2013, in preparation). For this smoother decline of the temperature profile, the nonthermal pressure contribution to the total support is consistent with that derived by simulations for relaxed clusters (see Lau et al. 2009; Vazza et al. 2011). These simulations show a radial increase of δ similar to that described by Equation (3) and a nonthermal pressure contribution to the total pressure of 30%–40% at the virial boundary. Greater values are obtained in the simulations of some relaxed clusters. A lower level of about 20% has been derived by the analysis of Morandi et al. (2012); a value that is also lower than the predictions from numerical simulations. This discrepancy may be due to their use of X-ray data limited at r_{500} where the steepening of the temperature profile observed by *Chandra* and *Suzaku* is not yet evident. A further cause is to consider spherical averaging of ellipsoidal galaxy clusters in the context of X-ray observables. However, the mean biases in observables are not greater than few percent within r_{500} (Buote & Humphrey 2012), although higher values are likely going toward the virial radius.

Mahdavi et al. (2013) found relaxed clusters consistent with no bias when hydrostatic and weak-lensing masses are compared

at r_{500}. However, we believe that the increasing radial profile of $p_{\rm nth}$ reported by the simulations may give hydrostatic masses that bias low at the virial radius. This is supported by the differences between $M_{\rm noturb}$ and $M_{\rm turb}$ at r_{500} and R in the relaxed A1835 (see Figure 3). This difference is negligible at r_{500} and is evident at R.

In summary, we have shown how the analysis of the X-ray observables allows us to derive a total mass profile consistent with the weak-lensing measurements, and to trace the thermal and nonthermal pressure profiles. This can be obtained by introducing in the HE equation a nonthermal pressure support as allowed by our SuperModel. In particular, we have reconstructed from *Chandra* X-ray observations the gas and total mass profiles of A1835. The values of δ_R and l which define the nonthermal pressure component have been obtained by the condition that $f_{\rm gas}$ equals $\Omega_b/\Omega_M - f_{\rm stars}$ at the virial radius. We have also shown that the level of turbulence δ_R depends on the observed ICP temperature profile. A steep drop in T implies a decreasing mass profile and therefore a high level of turbulence is required to obtain an increasing cluster mass profile that satisfies the cosmic gas mass fraction at the virial boundary. A lower level is necessary for a smoother decline of the temperature. This is consistent with the weakening of the accretion shocks that leads to a reduction of the thermal energy to feed the ICP entropy and to an increase of the bulk energy to drive turbulence in the cluster outskirts. As discussed in Section 2, the weakening degree of the accretion shocks may depend on the cluster environment and this seems to be confirmed by the significant azimuthal variations of the electron density, temperature, and entropy reported by *Suzaku* (Ichikawa et al. 2013). Using the SDSS photometric data for A1835 and A1689, the authors found that the hot regions are associated with a filamentary structure, while the cold regions contact low-density regions outside the clusters. Finally, the increasing $f_{\rm gas}$ profile at $r \gtrsim 0.3R$ reported in Figure 3 confirms the conclusion of Rasheed et al. (2010) that the baryons are not missing. They are simply located in the most peripheral regions of the clusters likely for the heating processes (such as shock heating of the gas, supernovae, and AGN feedback) that cause the ICP to expand or hinder its inflow.

We thank the referee for constructive comments. We are grateful to Massimiliano Bonamente for the submission of data on the *Chandra* brightness distribution and to Mauro Sereno for clarifying discussions. This work was supported by INAF and MIUR. A.L. thanks SISSA for warm hospitality.

REFERENCES

Afshordi, N., Lin, Y.-T., Nagai, D., & Sanderson, A. J. R. 2007, MNRAS, 378, 293
Akamatsu, H., Hoshino, A., Ishisaki, Y., et al. 2011, PASJ, 63, 1019
Arnaud, M., Pointecouteau, E., & Pratt, G. W. 2007, A&A, 474, L37
Battaglia, N., Bond, J. R., Pfrommer, C., & Sievers, J. L. 2012, ApJ, 758, 75
Bautz, M. W., Millwe, E. D., Sanders, J. S., et al. 2009, PASJ, 61, 1117
Bonamente, M., Landry, M., Maughan, B., et al. 2013, MNRAS, 428, 2812
Buote, D. A., & Humphrey, P. J. 2012, MNRAS, 421, 1399
Burns, J. O., Skillman, S. W., & O'Shea, B. W. 2010, ApJ, 721, 1105
Cavaliere, A., & Fusco-Femiano, R. 1976, A&A, 49, 137
Cavaliere, A., Lapi, A., & Fusco-Femiano, R. 2009, ApJ, 698, 580
Cavaliere, A., Lapi, A., & Fusco-Femiano, R. 2011, ApJ, 742, 19
Clowe, D., & Schneider, P. 2002, A&A, 395, 385
Dahle, H. 2006, ApJ, 563, 954
Ebeling, H., Edge, A. C., Bohringer, H., et al. 1998, MNRAS, 301, 881
Eckert, D., Ettori, S., Molendi, S., Vazza, F., & Paltani, S. 2013a, A&A, 551, A23
Eckert, D., Molendi, S., Vazza, F., Ettori, S., & Paltani, S. 2013b, A&A, 551, A22
Ettori, S., Morandi, A., Tozzi, P., et al. 2009, A&A, 501, 61
Fusco-Femiano, R., Cavaliere, A., & Lapi, A. 2009, ApJ, 705, 1019
Fusco-Femiano, R., Lapi, A., & Cavaliere, A. 2013, ApJL, 763, L3
Giodini, S., Pierini, D., Finoguenov, A., et al. 2009, ApJ, 703, 982
Gonzalez, A. H., Zaritsky, D., & Zabludoff, A. I. 2007, ApJ, 666, 147
Hinshaw, G., Larson, D., Komatsu, E., et al. 2013, ApJS, submitted (arXiv:1212.5226)
Hoekstra, H., Mahdavi, A., Babul, A., & Bildfell, C. 2012, MNRAS, 427, 1298
Hoshino, A., Henry, P. H., Sato, K., et al. 2010, PASJ, 62, 371
Iapichino, L., & Niemeyer, J. C. 2008, MNRAS, 388, 1089
Ichikawa, K., Matsushita, K., Okabe, N., et al. 2013, ApJ, 766, 90
Kawaharada, M., Okabe, N., Umetsu, K., et al. 2010, ApJ, 714, 423
Komatsu, E., Smith, K. M., Dunkley, J., et al. 2011, ApJS, 192, 18
Landry, M., Bonamente, M., Giles, P., Maughan, B., & Joy, M. 2012, MNRAS, submitted (arXiv:1211.4626)
Lapi, A., Fusco-Femiano, R., & Cavaliere, A. 2010, A&A, 516, 34
Lau, E. T., Kravtsov, A. V., & Nagai, D. 2009, ApJ, 705, 1129
Li, C. K., Jia, S. M., Chen, Y., et al. 2012, A&A, 545, 100
Mahdavi, A., Hoekstra, H., Babul, A., et al. 2013, ApJ, 767, 116
Mahdavi, A., Hoekstra, H., Babul, A., & Henry, J. P. 2008, MNRAS, 384, 1567
Metzler, C. A., & Evrard, A. E. 1994, ApJ, 437, 564
Morandi, A., Limousin, M., Sayers, J., et al. 2012, MNRAS, 425, 2069
Nagai, D., Kravtsov, A. V., & Vikhlinin, A. 2007a, ApJ, 668, 1
Nagai, D., Vikhlinin, A., & Kravtsov, A. V. 2007b, ApJ, 665, 98
Nagai, D., & Lau, E. T. 2011, ApJL, 731, L10
Planck Collaboration 2013a, A&A, submitted (arXiv:1303.5076)
Planck Collaboration 2013b, A&A, 550, A131
Rasheed, B., Bahcall, N., & Bode, P. 2010, PNAS, submitted (arXiv:1007.1980v1)
Rasia, E., Meneghetti, M., Martino, R., et al. 2012, NJPh, 14, 055018
Reese, E. D., Carlstrom, J. E., Joy, M., et al. 2002, ApJ, 581, 53
Sayers, J., Golwala, S. R., Ameglio, S., & Pierpaoli, E. 2011, ApJ, 728, 39
Schmidt, R. W., Allen, S. W., & Fabian, A. C. 2001, MNRAS, 327, 1057
Shaw, L. D., Nagai, D., Bhattacharya, S., & Lau, E. T. 2010, ApJ, 725, 1452
Simionescu, A., Allen, S. W., Mantz, A., et al. 2011, Sci, 331, 1576
Sun, M., Voit, G. M., Donahue, M., et al. 2009, ApJ, 693, 1142
Sunyaev, R. A., & Zeldovich, Ya. B. 1980, ARA&A, 18, 537
Tozzi, P., & Norman, C. 2001, ApJ, 546, 63
Umetsu, K., Birkinshaw, M., Liu, G.-C., et al. 2009, ApJ, 694, 1643
Valdarnini, R. 2011, A&A, 526, 158
Vazza, F., Brunetti, G., Gheller, C., & Brunino, R. 2010, NewA, 15, 695
Vazza, F., Brunetti, G., Gheller, C., Brunino, R., & Bruggen, M. 2011, A&A, 529, A17
Vazza, F., Eckert, D., Simionescu, A., Bruggen, M., & Ettori, S. 2013, MNRAS, 429, 799
Vikhlinin, A., Kravtsov, A., Forman, W., et al. 2006, ApJ, 640, 691
Voit, G. M. 2005, RvMP, 77, 207
Walker, S., Fabian, A., Sanders, J., & George, M. 2012a, MNRAS, 424, 1826
Walker, S., Fabian, A., Sanders, J., & George, M. 2012b, MNRAS, 427, 45
Walker, S., Fabian, A., Simionescu, A., & Tawara, Y. 2013, MNRAS, 432, 554
White, S. D. M., Navarro, J. F., Evrard, A. E., & Frenk, C. S. 1993, Natur, 366, 429
Zhang, Y.-Y., Finoguenov, A., Bohringer, H., et al. 2007, A&A, 467, 437
Zhang, Y.-Y., Okabe, N., Finoguenov, A., et al. 2010, ApJ, 711, 1033